Research Article

Lingyu Wang, Quan Chen, Zhongfa Zhou*, Xin Zhao, Jiancheng Luo, Tianjun Wu, Yingwei Sun, Wei Liu, Shu Zhang, and Wenhui Zhang

Crops planting structure and karst rocky desertification analysis by Sentinel-1 data

https://doi.org/10.1515/geo-2020-0272
received March 31, 2021; accepted July 06, 2021

Abstract: Accurate crop planting structure (CPS) information and its relationship with the surrounding special environment can provide strong support for the adjustment of agricultural structure in areas with limited cultivated land resources, and it will help regional food security, social economy, and ecological balance adjustment. However, due to the perennial cloudy, rainy, and scattered arable land in Karst mountainous areas, the monitoring of planting structure by traditional remote sensing methods is greatly limited. In this regard, we focus on synthetic aperture radar (SAR) remote sensing, which can penetrate clouds and rain, without light constraints to image. In this article, based on parcel-based temporal sequence SAR, the CPS in South China karst area was extracted by deep learning technology, and the spatial coupling relationship between CPS and karst rocky desertification (KRD) was analyzed. The results showed that: (a) The overall accuracy of CPS classification was 75.98%, which proved that the geo-parcel-based time series SAR has a good effect for the CPS mapping in the karst mountainous areas; (b) Through the analysis of the spatial relationship between the planting structure and KRD, we found that the lower KRD level caused the simpler CPS and the higher KRD grade caused more complex CPS and more richer landscape types. The spatial variation trend of CPS landscape indicates the process of water shortage and the deepening of KRD in farmland; (c) The landscape has higher connectivity (Contagion Index, CI 0.52–1.73) in lower KRD level and lower connectivity (CI 0.83–2.05) in higher KRD level, which shows that the degree of fragmentation and connection of CPS landscape is positively proportional to the degree of KRD. In this study, the planting structure extraction of crops under complex imaging environment was realized by using the farmland geo-parcels-based time series Sentinel-1 data, and the relationship between planting structure and KRD was analyzed. This study provides a new idea and method for the extraction of agricultural planting structure in the cloudy and rainy karst mountainous areas of Southwest China. The results of this study have certain guiding significance for the adjustment of regional agricultural planting structure and the balance of regional development.

Keywords: crop planting structure, time series SAR, karst, rocky desertification, farmland geo-parcels

1 Introduction

Agriculture is the foundation of social and economic development [1], and grain output is an important guarantee for social stability [2]. It affects the planning of national and regional economic development [3]. Crop planting structure (CPS) is one of the key factors affecting grain yield; it indicates the type of crops and its spatial distribution [4]. For a region, CPS means the relationship between food security and economic income [5]; however, the relationship between CPS and ecological environment receive little attention, and how these factors interact with each other remains an undefined question [6–8]. In order to clarify the problem, we selected the karst mountainous area in Southwest China, one of the three major karst concentrated distribution areas in the world [9], as the study area. In general, arable land resources are very scarce in karst mountainous areas around the world [10]. Different from

* **Corresponding author: Zhongfa Zhou,** School of Karst Science, School of Geography and Environmental Science, Guizhou Normal University, Guiyang 550001, China; State Engineering Technology Institute for Karst Desertification Control, Guiyang 550001, China, e-mail: fa6897@163.com
Lingyu Wang, Quan Chen, Xin Zhao, Shu Zhang, Wenhui Zhang: School of Karst Science, School of Geography and Environmental Science, Guizhou Normal University, Guiyang 550001, China
Jiancheng Luo, Yingwei Sun, Wei Liu: State Key Laboratory of Remote Sensing Science, Institute of Remote Sensing and Digital Earth, CAS, Beijing 100101, China
Tianjun Wu: School of Geology Engineering and Geomatics, Chang'an University, Xi'an 710064, China

the protection measures usually taken in similar fields in developed countries [11], as a large number of poor people live in China's karst mountainous areas, farmers often reclaim land on hillsides leading to massive soil erosion and karst rocky desertification (KRD) resulting in a fragile ecological environment and even natural disasters such as floods and mudflows [12,13]. Therefore, obtaining accurate CPS information and clarifying the relationship and rules between CPS and fragile ecological environment can better guide the adjustment of regional CPS, which is of great significance for balancing regional food security, farmers' income, and ecological benefits.

CPS mapping employ remote sensing, which is a relatively effective way to get the spatial distribution information due to the relatively large scale and high frequency acquisition of plant growth information [14,15]. This improves the limitations of traditional surveys and subsidiary decision of CPS optimization. In traditional classification methods, crops are classified based on optical images and used on a broad plain or global scale. A large number of studies applied Moderate Resolution Imaging Spectroradiometer data (normalized difference vegetation index, NDVI and enhanced vegetation index, EVI) [16,17] or Landsat [18] time series data to monitor the crops growth and recognize 2 or 3 types of crops such as rice, cotton, etc. However, the CPS means a combination of different types of crops; large scale remote sensing images cannot meet the extracting demand of complex type crops. With the development of earth observation and information technology [19], high-resolution remote sensing images provide sufficient data support for crops' classification [20,21]. But serious mixed pixel and lack of optical image data restricted these methods from being applied very well in South China karst area where the geological environment is extremely fragile [22] and perennial rainy. For example, in the center of SCK area, Guizhou province, the mountain area covered about 87% [23], and there are 1–2 effective optical images data can be collected, and the acquisition time of remote sensing image is not necessarily during the growing period of crops [24,25].

Many studies researched on how to avoid the errors caused by fragile landscape and focused on accurate ground object identification. Zhu et al. [26] and Deng et al. [27] increased the accuracy of the extracted winter wheat planting area based on field geo-parcels. Lv et al. compared the pixel-based, superpixel-based, and region-based classification methods, and they found that the region-based method had better segmentation accuracy and boundary fit, and solved the salt and pepper errors and low boundary adherence problems [28]. On the basis of farmland geo-parcels, some scholars extracted single planting types by overlaying time series data of parcels, and achieved good results [29–32]. Synthetic aperture radar (SAR) is considered to be one of the most important information sources for agricultural monitoring in cloudy and rainy regions due to the all-weather and all-day imaging capability [33]. Due to the complexity of SAR imaging mechanism, many scholars use SAR microwave remote sensing to sense the cultivated land underlying surface and try to extract a single category of crops, such as rice [34,35] and wheat [36–38], but it is difficult to identify the complex planting structures. In recent years, with the development of deep learning technology, some scholars have tried to carry out CPS classification of SAR remote sensing data with deep learning [15,39,40], and achieved good results.

In order to reveal the interaction and law between planting structure and rocky desertification, we tried to obtain accurate CPS information by using temporal series SAR data-based farmland geo-parcels, used the edge extraction method based on convolutional neural networks (CNN) to automatically extract the farmland plots, and used the recursive neural network (RNN) to identify the crop types. By overlaying the spatial distribution map of KRD grades, the spatial coupling relationship between KRD grades was analyzed, and the relationship between KRD and CPS was revealed to a certain extent. In order to guide the fine adjustment of CPS in karst mountainous areas and to balance the relations among regional food security, ecological benefits, and farmers' economic benefits, this article provides feasible ideas and methods.

2 Materials and methods

2.1 Study area

The study area shown in Figure 1 is located in Anshun city, Guizhou province, between 106°3′0″ E to 106°17′22″ E and 26°11′7″ N to 26°23′38″ N, covering an area of approximately 322.11 km². The climate of this region is the north subtropical monsoon humid climate with adequate rainfall. There are two sub-plains (cover area greater than 3.33 km²) in this area. Those are scarce resources in Guizhou province which is the only province in China without any plain. This area has a diverse karst and non-karst physiognomy.

2.2 Data

2.2.1 Multisource remote sensing images

There are three types of remote sensing images employed for this research: Google earth (GE) optical image data, Sentinel-1A SAR image data, and unmanned aerial vehicle

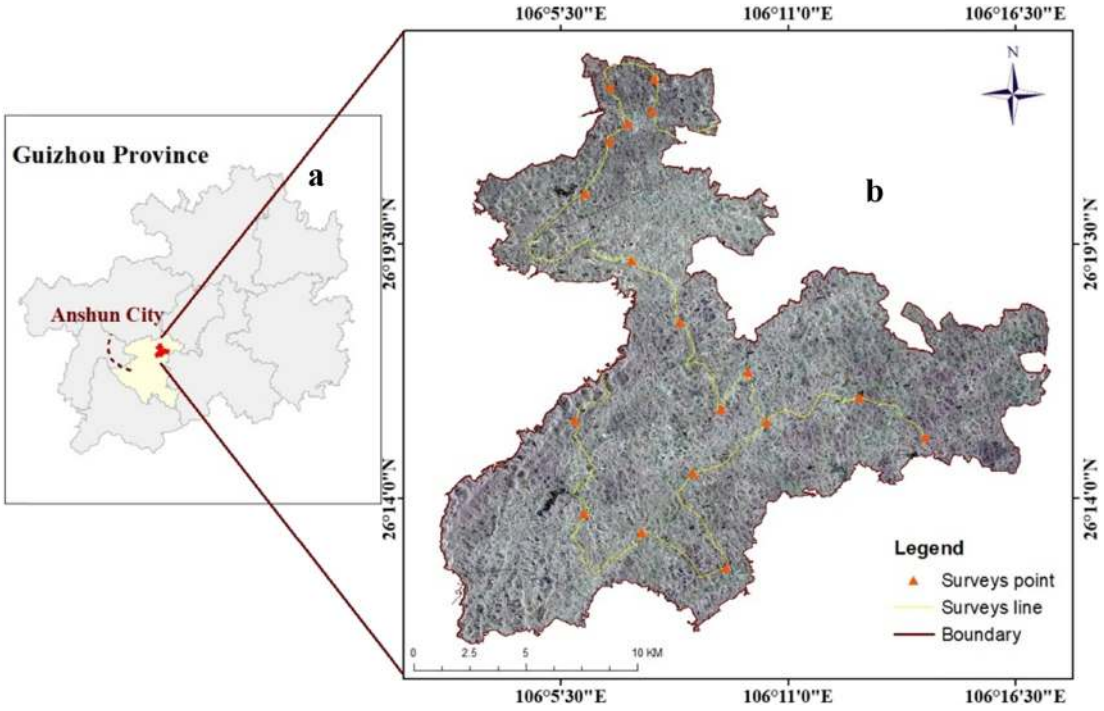

Figure 1: Location of the study area. (a) The location of study area in Anshun city, Guizhou province. (b) Details of study area based on Sentinel-1A SAR image taken on April 3, 2018.

(UAV) optical image data. We used GE image data which were downloaded from the website (https://earth.google.com/web/) for extracting farmland parcels; SAR data were download from ESA website (https://scihub.copernicus.eu) for crops classification; A number of UAV images which were captured during two field investigations, were randomly selected to make samples for training and the remaining were used for validation (Table 1).

The GE image consisted of mass different time pictures, the period of image download from Apr. 2018 to Aug. 2018; the farmland was barely changed.

Sentinel-1A containing four sensor modes has 20 m spatial resolution and two polarizations, VV and VH in C band. In this article, 12 images during crop growing seasons from Apr. 2018 to Aug. 2018 with IW mode and VV polarization were chosen for crop classification (Table 2).

The UAV images were captured by the Phantom 4 produced by DJI. In two field investigations, 3,172 UAV photos were captured from the UAV flies under the autopilot mode, which was pre-programmed with flight parameters such as altitude 120 m, side lap 80%, end lap 75%, and range.

2.2.2 Non-image data

In order to understand the distribution of crops better, geologic maps were employed for distinguishing the karst and non-karst area; the policy conditions and socioeconomic data can help in acquiring the crops planting information under policy orientation. The geologic maps were provided by the State Engineering Technology Institute for KRD. And the policy conditions and socioeconomic data such as Anshun statistical yearbook were downloaded from the web of Anshun people's government.

KRD grades can be considered as an index depended by slope, bare rock, soil erosion etc. Zhou et al. [41] and

Table 1: Details of multisource remote sensing images

Data type	Sensor	Data	Spatial resolution (m)	Band/polarization	Obtained from
Optical image	Google image	2018.4–2018.8	0.5	RGB	Web
	UAV	2018.8–2018.9	0.05	RGB	Field surveys
SAR image	Sentinel-1A	2018.4–2018.8	20	VV	Web

Table 2: Details of Sentinel-1A images

ID	Acquisition time	Polarization	ID	Acquisition time	Polarization
T1	03-04-2018	VV	T7	14-06-2018	VV
T2	15-04-2018	VV	T8	26-06-2018	VV
T3	27-04-2018	VV	T9	08-07-2018	VV
T4	09-05-2018	VV	T10	20-07-2018	VV
T5	21-05-2018	VV	T11	01-08-2018	VV
T6	02-06-2018	VV	T12	25-08-2018	VV

Li et al. [42] established standards for classifying KRD. In this article, we adopted the standard to classify the study area into eight areas and name them separately (Figure 2).

2.3 Processing

In ENVI 5.3, SAR images were preprocessed by data import, multi-looking, speckle filtering, geocoding, and radiometric calibration [39]. First, multi-looking produced the intensity images with VV and VH band. Second, speckle filtering was used for reducing the speckle noise. Third, geocoding was used to transfer the slant distance geometry into a geographic coordinate projection based on the selected digital elevation model, and the gray value of image was converted to a backscatter coefficient (dB). Finally, by exporting the SAR time series image dataset clipped by the boundary of study area, we got time sequence images. Through multiple experiments, the IW mode and VV polarization data presented the highest classification accuracy.

The UAV photos were preprocessed such as align photos, build mesh, three-dimensional triangulation, build point cloud, and mosaic photos, finally derived a total 18 ortho-images with 0.05 m spatial resolution, and investigated a total of 12,999 farmland parcels covering 13.68 km^2 (Table 3).

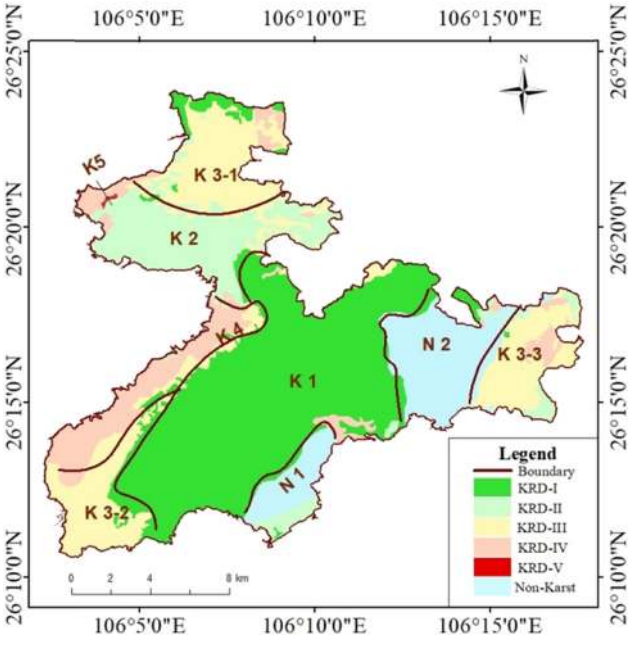

Figure 2: Partition of study area where 'N' stands for non-karst and 'K' stands for karst. The N1 and N2 represent the non-karst in study area. The K1–K5 represent KRD-I to KRD-V; K3-1, K3-2, and K3-3 indicate that there are three KRD-III areas distributed separately.

3 Methods

There are three steps for crop structure mapping: farmland parcels extraction, SAR time series construction, and crop classification. Then, transfer non-images data as KRD grades, policy conditions, and socioeconomic data to the parcels. Finally, coupling analysis of the relationship between KRD and crop structure is performed. The workflow of the crop structure mapping method is shown in Figure 3.

3.1 Software and map design

In this article, we employed Pix4D mapper software to preprocess the UAV data, and used ENVI 5.3 software to preprocess the Sentinel-1A SAR images. We accomplished the farmland parcels extraction and crop types identification with our own software. Then, all maps were made by using ArcMap10.2 software.

According to the morphological characteristics of the study area (Figure 4), we used a square composition. When designing the map, we fully considered the detailed presentation of the parcels-based planting structure. So,

Table 3: Details of UAV field surveys

	FLY ID	Parcel	Area (km^2)		FLY ID	Parcel	Area (km^2)
2018.8	081601	747	0.94	2018.9	091502-04	1,566	1.39
	081602-03	990	1.42		091505	613	0.79
	081604	1,238	1.00		091601-02	1,472	1.51
	081605	758	0.79		091603-04	718	0.81
	081606	1,517	1.37		091605-07	1,348	1.47
	081608	1,460	1.58		091609	572	0.61
Total		6,710	7.10	Total		6,289	6.58

we used partial magnification on the map to show the details.

3.2 Farmland parcels extraction Models

Three mature match networks were introduced to extract farmland parcel edges suitably in step one. Holistically-nested edge detection (HED) network was used for non-karst parcel extraction as the parcels' shape was inherently regular. For karst area, hilly farmland parcels were extracted by Dink-net network and inconsecutive parcels were extracted by U-net network.

3.2.1 HED

Using HED [43] network, the end-to-end edges were predicted; this network adds multiple side outputs and connects with the final convolution layer of each convolution pooling stage based on Visual geometry group network and then outputs edges of different scales. In this way, the results learned from each layer of the network are output through the side output layer, and a weighted fusion layer is adopted to utilize the results of these side outputs to realize the learning of multi-scale features of the image. In addition, edge features are continuously inherited and learned in the multi-layer network to finally get a more accurate

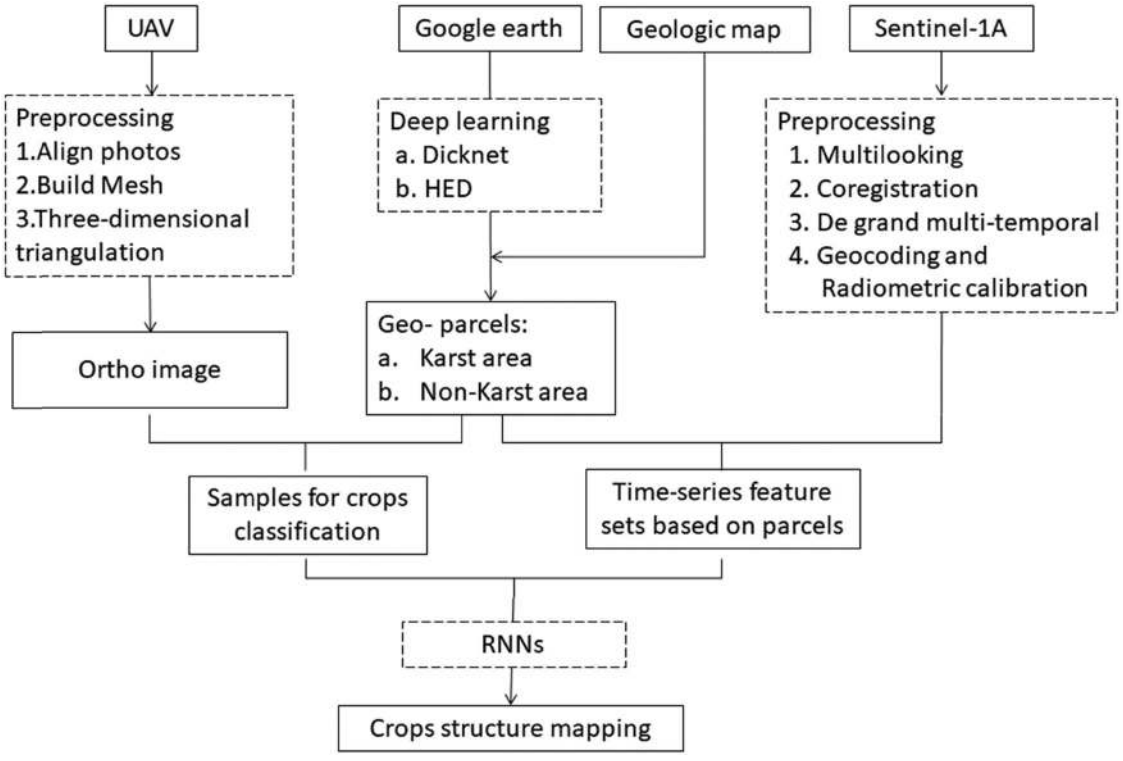

Figure 3: The workflow of the crop structure mapping.

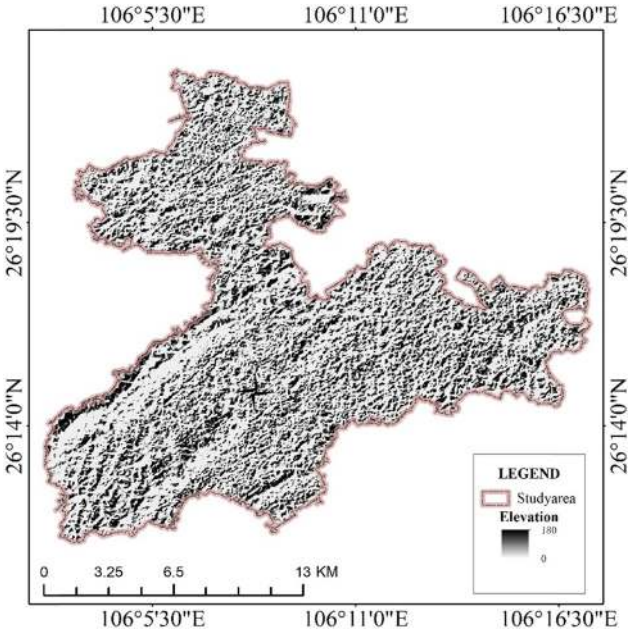

Figure 4: Geomorphological map of the study area.

farmland boundary line and then get regular farmland map spots through "line to polygon."

3.2.2 Dink-net

Due to the arbitrariness of the mountain farming in karst areas and the shielding effect of trees and weeds, the boundary is often not obvious. But these farmlands present unique texture and color features in the image. Thus, Dink-network is adopted to extract hilly farmlands.

3.2.3 U-net

U-net was originally applied to medical imaging procedures to improve the utilization of sample data to obtain an improved segmentation result with a small number of sample images. U-net can learn effective features by multiple layers from the sample dataset: sample image X and ground truth Y constitute patch (X, Y), and pixel i in image X and its label l, i in Y can be detected by filter kernels and explained as x_i. The L-layer network includes a series of nonlinear transforms and pool layers:

$$f(x_i) = w_l H_{l-1} + b_l, \quad l \in (1, \ldots, L), \tag{1}$$

where H_l is the covn layer l of the entire network, H_{l-1} is the pool layer, b_l is a bias term, and w_l is the parameter of layer l (Figure 5).

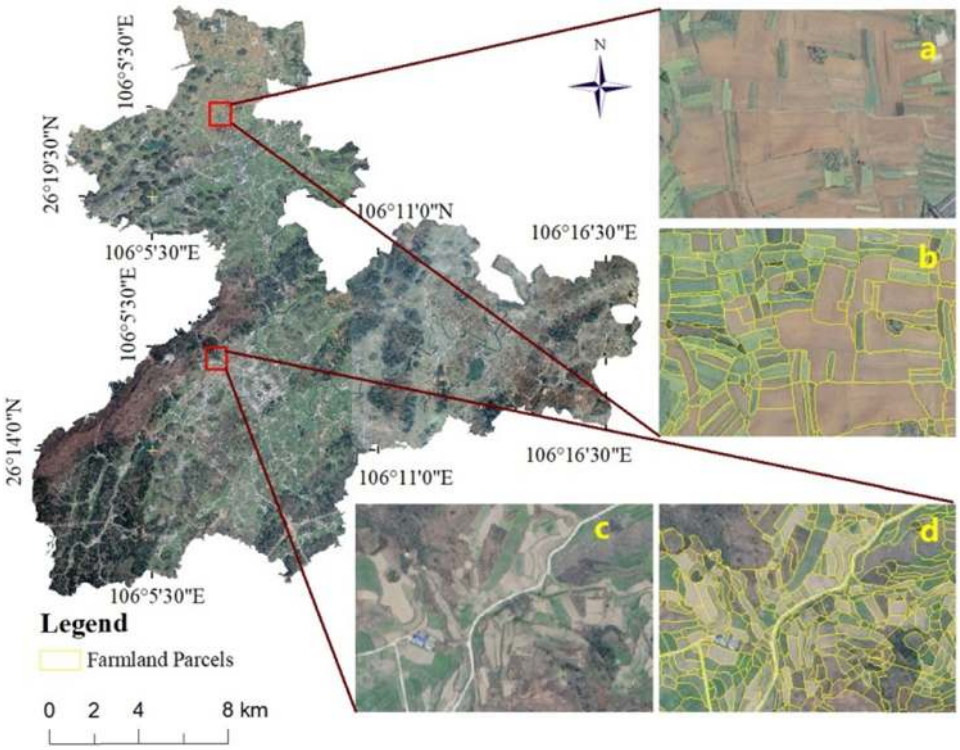

Figure 5: Extraction results of farmland parcels (partial). (a and c) Pre-extraction GE image; (b and d) results of farmland parcels extraction for (a) and (c).

3.3 Crop types identification

The farmland parcel layer was overlaid on SAR images; the mean intensity value of VV within each single parcel pixel was assigned to the corresponding parcel. Then, the VV intensity value of ten SAR images were assigned to the parcels one by one, and finally, the time series parcels for crop type identification were constructed.

RNNs are designed to learn features from sequence datasets, and they perform well in signal processing and speech transformation [44,45]. Compared with CNNs, RNNs mainly consider the contextual information of the sequence, which means that every state's input covers the output of the previous state [46–48]. In this study, an RNN structure with long short-term memory (LSTM) [49] units is used to learn the features from the established time series of optical and SAR datasets to classify crops.

In this article, we selected the stack type to realize the classification task. The deep architecture consists of six LSTM layers for extracting high-level nonlinear time characteristics from multitemporal remote sensing datasets. Moreover, another *SoftMax* layer was stacked on the last unit to perform the multiclass prediction, and this layer has the same number of neurons as the class number. This structure allows every hidden layer to determine the features on different time scales.

3.4 Crop type structure analysis using landscape theory

Landscape has multi-characteristics such as diversity, function, and scarcity, and these were descripted in land space by patch of ecologic system. In this article, we employed the landscape indices such as percentage of landscape (PLAND), mean patch size (MPS), and CI, to describe the crops distribution as types and scales and then combined them to draw the landscape structure containing CPS, spatial heterogeneity, and the correlation with KRD.

PLAND was used for expressing the total percentage of a certain crop type's area. The higher the value was, the larger the type of coverage. The formula for the PLAND calculation is shown in equation (2):

$$\text{PLAND} = \sum_{i=1}^{n} a_{ij}/A \times 100. \tag{2}$$

CI and MPS were employed to draw the fragment of certain type. They are reciprocal to each other, but CI expresses the mean parcel size and MPS shows the number of parcels in certain zone. The formulas for the CI and MPS calculation are shown in equations (3 and 4):

$$\text{MPS} = \sum_{i=1}^{n} a_{ij}/N_j, \tag{3}$$

$$\text{CI} = N_j \Big/ \sum_{i=1}^{n} a_{ij}. \tag{4}$$

In the formulas (1)–(4), a is the area value; i is the parcels' number (from 1 to n); j is the crop type; A is the sum of areas of farmland in study area; N is the sum of number of farmland parcels.

4 Results and analysis

4.1 Results of farmland parcels extraction and crops classification

There are 270,833 parcels that were extracted and cover 20897.19 ha. Of these, 234,780 parcels (17893.86 ha) are

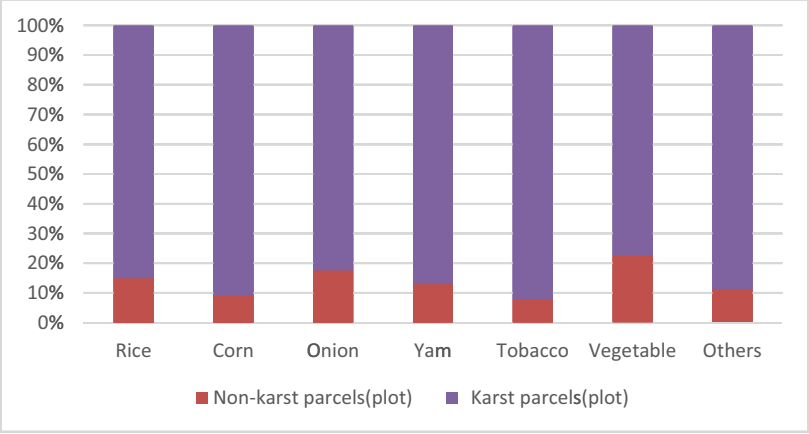

Figure 6: The proportions of various crops in karst and non-karst areas.

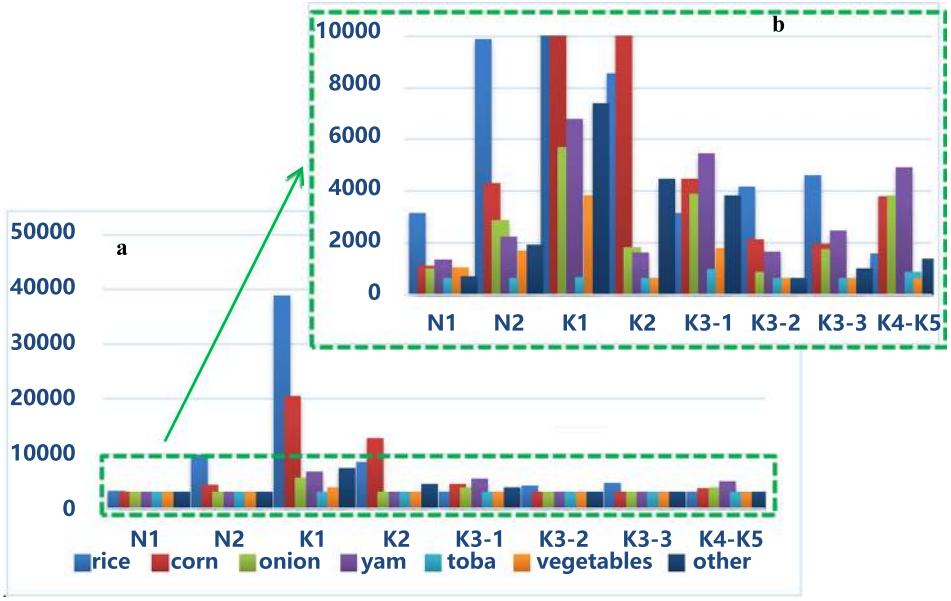

Figure 7: CPS composition of different areas: (a) total CPS composition of different areas; (b) detail of (a).

situated within karst area, the rest 36,053 parcels (3003.33 ha) are situated within Non-karst area. According to SAR time series, farmland parcels were divided into seven crop types: rice (35%), corn (24%), onion (11%), yam (13%), tobacco (2%), vegetables (5%), and others (10%). The crops in the study area are mainly distributed in the karst area (86.68%), and only 13.32% are distributed in the non-karst area (Figures 6 and 7) (Table 4).

4.2 Evaluation

We used six UAV images data for manual visual interpretation, and compared with the extracted planting type. The crop classification results of the accuracy assessment are as follows: the rice is 86.14%, the corn is 78.96%, the onion is 89.13%, the yam is 64.53%, the tobacco is 68.17%, the vegetables are 71.44%, and others are 73.5%. The overall accuracy is 75.98%.

4.3 Landscape analysis of CPS types

According to the proportion and distribution of the planting structure in the study area, the planting types with the PLAND index of the planting structure greater than 20% were selected as the main landscape in the region, and the planting types with the PLAND index greater than 30% were selected as the absolute dominant landscape [50]. Therefore, these areas were divided into groups with different planting structures: the absolute dominant CPS landscape of N1, N2, and K1 was “rice,”

Table 4: Quantity and area of various crops in karst and non-karst areas

	Non-karst		Karst		Total	
	Area (ha)	Parcels (plot)	Area (ha)	Parcels (plot)	Area (ha)	Parcels (plot)
Rice	1196.93	14,167	6212.08	80,867	7409.01	95,034
Corn	525.70	6,412	4600.34	64,244	5126.05	70,656
Onion	388.65	4,588	1802.90	21,594	2191.54	26,182
Yam	343.31	4,493	2319.17	30,251	2662.48	34,744
Tobacco	41.10	299	331.07	3,586	372.16	3,885
Vegetable	250.46	3,069	767.91	10,400	1018.37	13,469
Others	257.18	3,025	1860.40	23,838	2117.58	26,863
Total	3003.33	36,053	17893.86	234,780	20897.19	270,833

Table 5: CI values of different crops in different areas

CI (/ha)	N1	N2	K1	K2	K3-1	K3-2	K3-3	K4-K5
rice	1.25	1.18	1.24	1.40	1.37	1.57	1.24	1.61
corn	1.22	1.23	1.28	1.43	1.23	1.83	1.38	1.86
onion	1.07	1.23	1.24	1.48	1.07	1.37	1.13	1.12
yam	1.19	1.37	1.34	1.57	1.08	1.49	1.19	1.40
tobacco	0.52	1.18	1.10	1.15	0.83	1.45	0.90	1.34
vegetables	1.13	1.24	1.30	1.52	1.10	2.05	1.56	2.02
other	1.23	1.20	1.32	1.40	1.00	1.52	1.25	1.41

Table 6: MPS values of different crops in different areas

MPS (ha)	N1	N2	K1	K2	K3-1	K3-2	K3-3	K4-K5
rice	0.80	0.85	0.81	0.71	0.73	0.64	0.80	0.62
corn	0.82	0.81	0.78	0.70	0.81	0.55	0.72	0.54
onion	0.93	0.82	0.81	0.68	0.93	0.73	0.89	0.90
yam	0.84	0.73	0.74	0.64	0.92	0.67	0.84	0.71
tobacco	1.93	0.85	0.91	0.87	1.21	0.69	1.11	0.75
vegetables	0.88	0.81	0.77	0.66	0.91	0.49	0.64	0.49
other	0.81	0.84	0.76	0.72	1.00	0.66	0.80	0.71

the PLAND indices are 36.52, 42.82, and 46.38%, respectively; the dominant CPS of K2–K5 was "corn," the PLAND indices are 32.60% (K2), 30.99% (K3-1), 42.05% (K3-2), 33.57% (K3-3), and 29.37% (K4-K5). The main landscape of N1, N2, and K1 was "rice;" the main landscape of K2 and K3 was "rice-corn," the sum of the PLAND indices are 60.90% (K2), 44.29% (K3-1), 64.92% (K3-2), and 52.31% (K3-3); the main landscape of K4 and K5 was "corn-onion-yam," the PLAND indices are 29.37% (corn), 22.63% (onion), and 22.09% (yam).

The CI and MPS values are shown in Tables 5 and 6. On the whole, the crops planting size of N1–K1 is relatively uniform, while K2–K5 show great differentiation and the landscape fragmentation increases. From a single point, the CI of K2, K3-2, and K4–K5 are generally high, and the MPS are low. These indicate that landscapes were broken in these areas. On the contrary, the parcels of N1, N2, and K1 with low CI and high MPS were highly connected.

From the other point of view, the degree of the tobacco landscape is the best. In the non-karst area, the landscape of rice, corn, and onion is gradually dispersed. In the karst area, especially the K2–K4, the rice, corn, and vegetables with high CI and low MPS, it can be inferred that the landscapes were fragmented and heterogeneous.

The graph also shows some patterns; the landscape has the high connectivity in N1–K1, the value of CI ranges from 0.52 to 1.73 and the landscape becomes discrete and fragmented from K2 to K4, the value of CI ranges from 0.83 to 2.05. But K3-1 rendering features as shown from Figure 8 the landscape was connective and the size was equalization. Such differences also appear in the tables and figures: the CI value were maintained a lower level, presents a trough compared with K2 and K3-2 (Figure 9 and 10).

4.3.1 Coupling analysis of the crops' spatial structure and KRD spatial distribution

Based on the above analysis of the planting structure landscape and rocky desertification (Figure 11), we summarized the following coupling relationship between the planting structure space and KRD space.

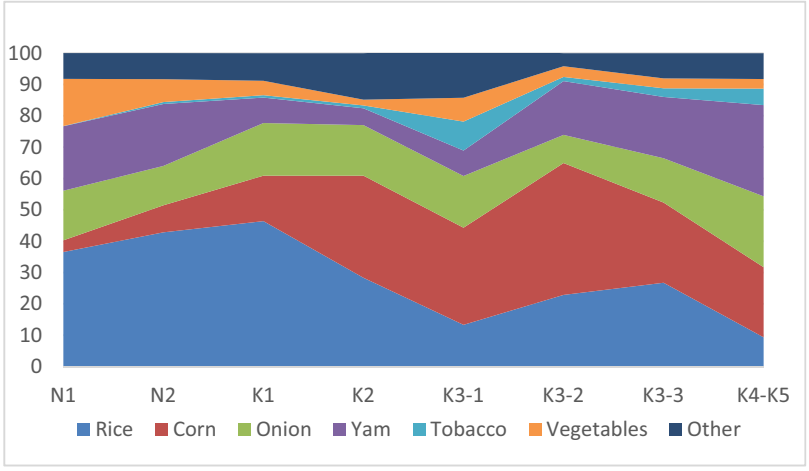

Figure 8: PLAND value with different crop types in different areas.

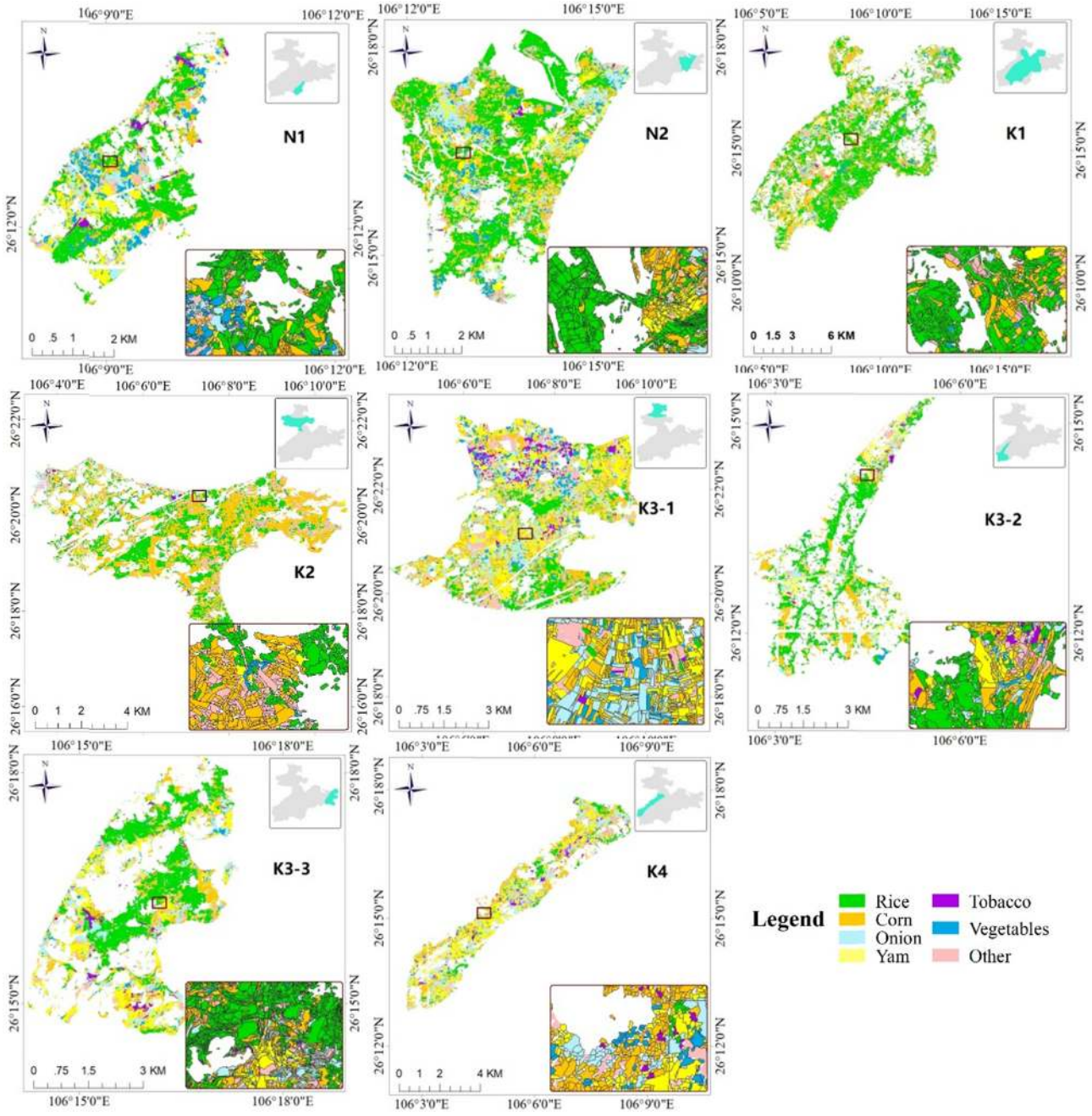

Figure 9: CPS composition map of N1 to K4; in the upper left corner of each image is the location of the image in the study area; the red box in each image shows the randomly selected range and its enlarged image.

Based on the analysis of the landscape distribution of the main planting structures in the regions with different grades of rocky desertification, the PLAND index of rice was K1 > N2 > N1 > K3 > K4–5, corn PLAND index was K3 > K2 > K4–5 > K1 > N2 > N1, onion PLAND index was K4–5 > K3 > K2 > K1 > N1 > N2, yam PLAND index was K4–5 > K3 > N2 > N1 > K1, etc. Meanwhile, ranking of CI index of rice in each KRD was N2 < N1 < K1 < K2 < K3 < K4–5, the corn was N1 < N2 < K1 < K2 < K3 < K4–5, the onion was N1 < N2 < K1 < K3 < K4–5 < K2, and the yam was N1 < K3 < K1 < N2 < K4–5 < K2. The structure landscape dominated by rice gradually transitioned to corn, onion, yam etc., from N1 to K5. The landscape based on farmland parcels, it is the performance that paddy field transitions dryland. This feature is well verified: with the increase in rocky desertification grade, the proportion of

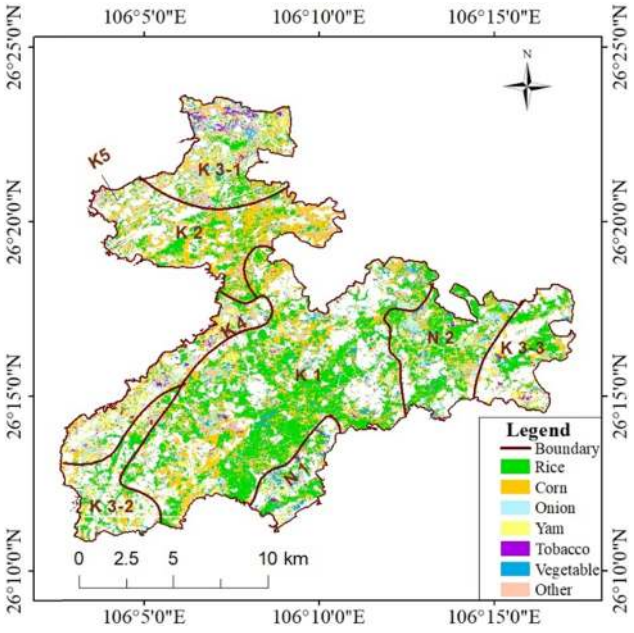

Figure 10: Crops' spatial structure and KRD spatial distribution.

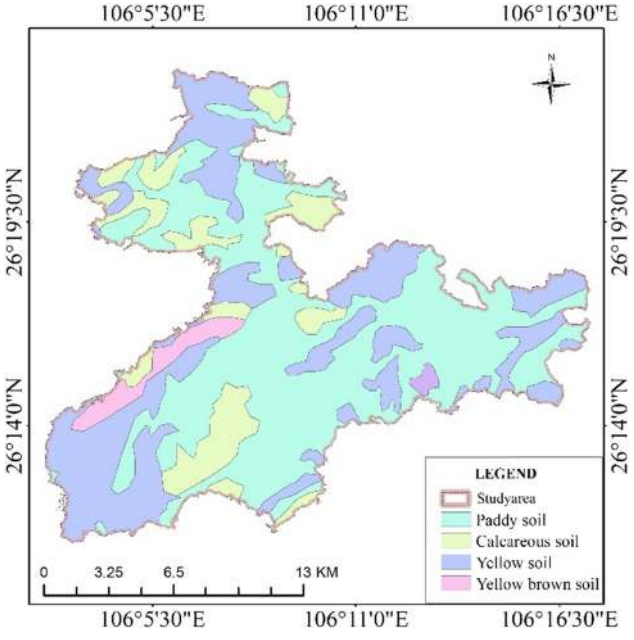

Figure 11: Soil type map of the study area.

paddy field decreased and the proportion of dryland crops increased.

In the study area, rice is the absolutely dominant landscape in non-karst area and slight KRD area (PLAND >30%). With the decrease in dominant food crop landscape, the proportion of other crops landscape increased, and the landscape type of planting structure in the area became richer. As can be seen from Table 3, from N1 to K4, the landscape proportion of rice and corn decreased from 62 to 32%, and the landscape proportion of non-food crops such as yam, green onion, and vegetables increased from 30 to 60%. We can conclude that the lower KRD level caused the simpler crop structure, as the KRD grade increased, the fragmentation and heterogeneity of farmland were increased, causing the more complex crop structure and more richer landscape types.

KRD caused the fragmentation of the planting landscape. Combined with the existing research results, soil moisture is the difference between paddy field and dryland landscape [51]. With the deepening of rocky desertification, soil moisture also decreases gradually, which reflects the degree of rocky desertification [52]. It can be concluded that the landscape of planting structure gradually changed from rice to dryland crops structure with the increase in the rocky desertification. This pattern of change in the planting structure testifies to the degree of water scarcity in the land.

5 Conclusion

The environmental suitability of crops is crucial to the adjustment of planting structure in karst mountainous areas. In the past, there have been a lot of studies on using optical satellite images to draw crop maps. However, due to the limitations of mountainous terrain and climate, there were problems such as difficulty in obtaining optical remote sensing data sources, mixing image elements, and salt and pepper noise. To solve these problems, our research focused on the identification of planting structure based on farmland geo-parcels and the analysis of the coupling relationship between planting structure and geographical environmental background.

We used GE high-resolution image to obtain the boundary of the block, and constructed a time series dataset from the SAR microwave image of the Sentinel-1 satellite. Considering the farmland geo-parcel's characteristics and crop growth characteristics in karst mountainous areas, we have made a large number of cultivated land and crop type samples. According to different terrain backgrounds, different segmentation models were used to extract the cultivated land boundary and then the crops were classified by using RNNs network in the time series dataset at the parcel level, which achieved a good accuracy. We demonstrated the great potential of SAR in the identification of implant structures.

Combined with some geographical background data, we analyzed the relationship between the planting

structure and the rocky desertification environment. From the perspective of landscape science, some conclusions are drawn: the paddy field size is inversely correlated with the degree of rocky desertification; the landscape size of dryland crops is positively correlated with the degree of rocky desertification; The increase in the corn landscape often indicates a more fragmented landscape. Fewer rice landscapes often mean more complex and fragmented landscapes. Our results indicated that the planting structure indicates the extent of rocky desertification to some extent. There is a mutual influence and restriction on each other, human intervention plays a guiding role in this relationship.

There are still some limitations in this study. On the one hand, farmers are the determinants of the planting types, and farmers' decisions depend on the environmental suitability of crops and the judgment of economic market. Our study only analyzed the limitations of natural environment. On the other hand, this study mainly focuses on the information acquisition and analysis of large-scale satellite remote sensing and land parcel scale. Under sufficient conditions, it can combine with more microscopic ground sample (soil, water, etc.) analysis to obtain more accurate results to guide production. These questions will be studied in our future work.

Acknowledgments: We appreciate the Image Sky International Co. Ltd. for providing hardware and software support.

Funding information: This work was supported by the National Natural Science Foundation of China, (Grant No. 41661088, 41631179, and 41601437); the National Key Research and Development Program of China (Grant No. 2017YFB0503600); Research Fund for Postgraduates of Guizhou Province (Grant No. YJSCXJH (2020) 103); Science and Technology Plan Program in Guizhou Province (Grant No. 2017-5726-57); High-level Innovative Talents Training Program in Guizhou Province (Grant No. 2016-5674).

Conflict of interest: The authors declare that there is no conflict of interest regarding the publication of this paper.

References

[1] Johnston BF, Mellor JW. The role of agriculture in economic development. Am Econ Review. 1961;51(4):566–93.

[2] Wang H, Zhang M, Cai Y. Problems, challenges, and strategic options of grain security in China. Adv Agron. 2009;103:101–47.

[3] Timmer CP. Agriculture and economic development. Handb Agric Econ. 2002;2:1487–546.

[4] Tang HJ, Wu WB, Yang P, Zhou QB, Chen ZX. Recent progresses in monitoring crop spatial patterns by using remote sensing technologies. Sci Agric Sin. 2010;43(14):2879–88. (in Chinese).

[5] Yin PH, Fang XQ, Ma YL, Tian Q. New regional pattern of grain supply-demand in China in the 21st century. J Nat Resour. 2006;4:625–31 + 678.

[6] Liu ZH, Yang P, Wu WB, Li ZG, You LZ. Spatio-temporal changes in Chinese crop patterns over the past three decades. Acta Geogr Sin. 2016;71(5):840–51.

[7] Qingfeng Z, Jian W, Longshan Z. M-DEM-based micro-topography characteristics of artificial tillage loess slope. J Arid Land Resour Environ. 2012;26(9):149–53.

[8] Shui W, Chen Y, Su Z, Fan S. Agricultural ecosystem services function value evaluation under the influence of specialized tea planting: a case study in Anxi, Fujian Province. Acta Ecol Sin. 2017;37(10):3311–26.

[9] Ford DC, Williams PW. Karst geomorphology and hydrology. London: Unwin Hyman; 1989.

[10] Peng T, Wang S. Effects of land use, land cover and rainfall regimes on the surface runoff and soil loss on karst slopes in Southwest China. Catena. 2012;90:53–62.

[11] Wang SJ, Zhang DF, Li RL. Mechanism of rocky desertification in the karst mountain areas of Guizhou province, Southwest China. Int Rev Environ Strat. 2002;3(1):123–35.

[12] Li RL, Wang SJ, Zhou DQ. Correlation between rocky desertification and slope degree in Karst area of Guizhou. Bull Soil Water Conserv. 2006;4:82–6.

[13] Su W. Soil erosive deterioration and its control in Karst mountainous regions of Guizhou province. Carsol Sin. 2001;3:51–7.

[14] Xiao X, Boles S, Frolking S, Li C, Babu JY, Salas W, et al. Mapping paddy rice agriculture in South and Southeast Asia using multi-temporal MODIS images. Remote Sens Environ. 2006;100(1):95–113.

[15] Sun Y, Luo J, Wu T, Zhou Y, Liu H, Gao L, et al. Synchronous response analysis of features for remote sensing crop classification based on optical and SAR time-series data. Sensors. 2019;19(19):4227.

[16] Brown JC, Kastens JH, Coutinho AC, Victoria DDC, Bishop CR. Classifying multiyear agricultural land use data from Mato Grosso using time-series MODIS vegetation index data. Remote Sens Environ. 2013;130:39–50.

[17] Wardlow B, Egbert S, Kastens J. Analysis of time-series MODIS 250 m vegetation index data for crop classification in the US central great plains. Remote Sens Environ. 2007;108(3):290–310.

[18] Foerster S, Kaden K, Foerster M, Itzerott S. Crop type mapping using spectral-temporal profiles and phenological information. Comput Electron Agric. 2012;89:30–40.

[19] Bruzzone L, Carlin L. A multilevel context-based system for classification of very high spatial resolution images. IEEE Trans Geosci Remote Sens. 2006;44(9):2587–600.

[20] Lv X, Ming D, Lu T, Zhou K, Wang M, Bao H. A new method for region-based majority voting CNNs for very high resolution image classification. Remote Sens. 2018;10(12):1946.
[21] Yang C, Everitt JH, Murden D. Evaluating high resolution SPOT 5 satellite imagery for crop identification. Comput Electron Agri. 2011;75(2):347–54.
[22] Blaschke T. Object based image analysis for remote sensing. ISPRS J Photogr Remote Sens. 2010;65(1):2–16.
[23] Blaschke T, Hay GJ, Kelly M, Lang S, Hofmann P, Addink E, et al. Geographic object-based image analysis – towards a new paradigm. ISPRS J Photogr Remote Sens. 2014;87:180–91.
[24] Zhang Y, Rossow WB, Lacis AA, Oinas V, Mishchenko MI. Calculation of radiative fluxes from the surface to top of atmosphere based on ISCCP and other global data sets: Refinements of the radiative transfer model and the input data. J Geophys Res Atmos. 2004;109(D19105):D19105.
[25] Hai X. Land cover classification in cloudy and hilly regions based on optical and SAR data. M.S. thesis, Southwest University, China; 2018.
[26] Zhu C, Luo J, Shen Z, Cheng X. Winter wheat planting area extraction using multi-temporal remote sensing data based on field parcel characteristic. Trans CSAE. 2011;27(9):94–9.
[27] Deng L, Shen Z, Ke Y, Xu Z. Winter wheat planting area extraction using multi-temporal remote sensing images based on field parcel. Trans CSAE. 2018;34(21):157–64.
[28] Lv X, Ming D, Lu T, Zhou K, Wang M, Bao H. A new method for region-based majority voting CNNs for very high resolution image classification. Remote Sens. 2018;10(12):1946.
[29] Guo L, Wang T, Wu Z, Wang J, Wang M, Cui Z, et al. Accurate recognition and extraction of Karst abandoned land features based on cultivated land plot and time series NDVI. Remote Sens Land Resour. 2020;32(3):23–31.
[30] Yin H, Prishchepov AV, Kuemmerle T, Bleyhl B, Buchner J, Radeloff VC. Mapping agricultural land abandonment from spatial and temporal segmentation of Landsat time series. Remote Sens Environ. 2018;210:12–24.
[31] Yang Y, Huang Q, Wu W, Luo J, Gao L, Dong W, et al. Geo-parcel based crop identification by integrating high spatial-temporal resolution imagery from multi-source satellite data. Remote Sens. 2017;9:1298.
[32] Wang LY, Zhou ZF, Zhao X, Kong Jie, Zhang Shu. Temporal and spatial evolution of karst rocky desertification abandoned cropland based on time series remote sensing and cultivated land plot. J Soil Water Conserv. 2020;34(1):92–99 + 107.
[33] Jiao X, Kovacs JM, Shang J, McNairn H, Dan W, Ma B, et al. Object-oriented crop mapping and monitoring using multi-temporal polarimetric RADARSAT-2 data. ISPRS J Photogr Remote Sens. 2014;96:38–46.
[34] Li H, Fu D, Huang C, Su F, Liu Q, Liu G, et al. An approach to high-resolution rice paddy mapping using time-series Sentinel-1 SAR data in the Mun River Basin, Thailand. Remote Sens. 2020;12(23):3959.
[35] Subbarao NVT, Mani JK, Shrivastava A, Srinivas K, Varghese AO. Acreage estimation of kharif rice crop using Sentinel-1 temporal SAR data. Spat Inf Res. 2020:1–11.
[36] Mouret F, Albughdadi M, Duthoit S, Kouamé D, Rieu G, Tourneret JY. Outlier detection at the parcel-level in wheat and rapeseed crops using multispectral and SAR time series. Remote Sens. 2021;13(5):956.
[37] Nasrallah A, Baghdadi N, Hajj ME, Darwish T, Belhouchette H, Faour G, et al. Sentinel-1 data for winter wheat phenology monitoring and mapping. Remote Sens. 2019;11(19):2228.
[38] Cai W, Zhao S, Wang Y, Peng F, Heo J, Duan. Z. Estimation of winter wheat residue coverage using optical and SAR remote sensing images. Remote Sens. 2019;11(10):1163.
[39] Zhou Y, Luo J, Feng L, Yang Y, Chen Y, Wu W. Long-short-term-memory-based crop classification using high-resolution optical images and multi-temporal SAR data. GISci Remote Sens. 2019;56(8):1170–91.
[40] Liu W, Wang J, Luo J, Wu Z, Chen J, Zhou Y, et al. Farmland parcel mapping in mountain areas using time-series SAR data and VHR optical images. Remote Sens. 2020;12(22):3733.
[41] Zhou ZF, Yan LH, Chen Q. Evolution mechanism and regulation of karst rocky desertification under human intervention. Beijing: Science Press; 2016.
[42] Li RL, Wang SJ, Zhou DQ. Correlation between rocky desertification and slope degree in Karst area of Guizhou. Bull Soil Water Conserv. 2006;4:82–6.
[43] Xie S, Tu Z. Holistically-nested edge detection. Int J Comput Vis. 2017;125(1–3):3–18.
[44] Soma K, Mori R, Sato R, Furumai N, Nara S. Simultaneous multichannel signal transfers via chaos in a recurrent neural network. Neural Comput. 2015;27(5):1083–101.
[45] Linzen T, Dupoux E, Goldberg Y. Assessing the ability of LSTMs to learn syntax-sensitive dependencies. Trans Assoc Comput Linguist. 2016;4:521–35.
[46] Zhang Y, Tang J, Liao R, Zhang M, Zhang Y, Wang X, et al. Application of an enhanced BP neural network model with water cycle algorithm on landslide prediction. Stoch Environ Res Risk Assess. 2021;35(6):1273–91.
[47] Zhang Y, Tang J, He Z, Tan J, Li C. A novel displacement prediction method using gated recurrent unit model with time series analysis in the Erdaohe landslide. Nat Hazards. 2021;105(1):783–813.
[48] Zhang Y, Chen X, Liao R, Liao RP, Wan JL, He ZY, et al. Research on displacement prediction of step-type landslide under the influence of various environmental factors based on intelligent WCA-ELM in the Three Gorges Reservoir area. Nat Hazards. 2021;107(2):1709–29.
[49] Hochreiter S, Schmidhuber J. LSTM can solve hard long time lag problems. Adv Neural Inf Process Syst. 1997;473–9.
[50] Provost GL, Badenhausser I, Violle C, Requier F, D'Ottavio M, Roncoroni M, et al. Grassland-to-crop conversion in agricultural landscapes has lasting impact on the trait diversity of bees. Landsc Ecol. 2020;36:281–95. (prepublish).
[51] Chen HS, Wang KL. Soil water research in Karst mountain areas of Southwest China. Res Agric Modern. 2008;29(6):734–8.
[52] Chen Q, Zhou ZF, Wang LY, Dan YS, Tang YT. Surface soil moisture retrieval using multi-temporal Sentinel-1 SAR data in karst rocky desertification area. J Infrared Millim Waves. 2020;39(5):626–34.